JOURNAL OF MAGNETIC RESONANCE **124,** 223–226 (1997)
ARTICLE NO. MN961008

# Observations of Diffusive Diffraction in a Cylindrical Pore by PFG NMR

STEPHEN J. GIBBS

*Center for Interdisciplinary Magnetic Resonance, National High Magnetic Field Laboratory, Florida State University, 1800 East Paul Dirac Drive, Tallahassee, Florida 32310; and Department of Chemical Engineering, FAMU-FSU College of Engineering, 2525 Pottsdamer Street, Tallahassee, Florida 32307*

Received September 16, 1996

Pulsed-field-gradient (PFG) NMR observations of spatial restrictions to diffusion have great potential for aiding spatial structure determination in a wide variety of porous media. Some practical examples of current interest include the noninvasive determination of nerve fiber orientation and size, characterization of pore sizes and permeability in oil-bearing rock formations, and structure and transport property determination in packed beds and other porous media of use in chemical reaction engineering and separation processes.

Toward these ends, several important advances in the theory of PFG NMR measurements on systems exhibiting restricted diffusion have been published in the past few years (*1–8*). Recently, Callaghan (*1*) has published exact, analytical expressions for the echo attenuation in planar, cylindrical, and spherical pores valid for conditions of short gradient pulses and possible wall or surface-induced relaxation. The present note describes a comparison of experimental PFG NMR data for a water-filled cylinder and the analytical treatment (*1*).

For restricted geometries and long diffusion times, PFG NMR data exhibit *diffusive diffraction;* destructive interference of magnetization contributing to the echo occurs at particular values of the product $qa$, where $q = \gamma g \delta/2\pi$, $\gamma$ is the magnetogyric ratio of the observed nucleus, $\delta$ is the duration of the magnetic-field-gradient pulses for motion encoding, $g$ is the applied pulsed gradient, and $a$ is a characteristic dimension of the restricted geometry. This behavior may prove useful for the characterization of the length scales and geometries of restrictions to diffusion in porous media.

For the specific case of restricted diffusion in a cylindrical geometry with the pulsed field gradients oriented orthogonal to the axis of the cylinder, Callaghan found that (*1*)

$$E(q,\Delta) = \sum_k \frac{4\beta_{0k}^2 \exp[-\beta_{0k}^2 D\Delta/a^2][(2\pi qa)J_0'(2\pi qa) + (Ma/D)J_0(2\pi qa)]^2}{[(Ma/D)^2 + \beta_{0k}^2][(2\pi qa)^2 - \beta_{0k}^2]^2} + \sum_{nk} \frac{8\beta_{nk}^2 \exp[-\beta_{nk}^2 D\Delta/a^2][(2\pi qa)J_n'(2\pi qa) + (Ma/D)J_n(2\pi qa)]^2}{[(Ma/D)^2 + \beta_{nk}^2 - n^2][(2\pi qa)^2 - \beta_{nk}^2]^2}, \quad [1]$$

where $E(q, \Delta)$ is the echo amplitude relative to the amplitude at $q = 0$ as a function of the magnitude of the wave vector for motion encoding $q$ and the diffusion time $\Delta$, the $J_n$ are the standard (cylindrical) Bessel functions, the $\beta_{nk}$ are given by

$$\beta_{nk}J'(\beta_{nk})/J_n(\beta_{nk}) = -Ma/D, \quad [2]$$

$a$ is the cylinder radius, $D$ is the diffusion coefficient of the observed species, and $M$ is the surface relaxivity of the cylinder walls.

We report below a favorable comparison of Eq. [1] and experimental data obtained from PFG NMR measurements on a water-filled 100 $\mu$m i.d. capillary tube.

Measurements were performed with a Bruker Avance DMX spectrometer operating at 600 MHz for protons and coupled with a 14 T, 89-mm-bore Bruker/Magnex magnet. This system is equipped with an actively shielded gradient set capable of 0.96 T/m at 40 A.

Precision-bore glass capillaries (i.d. 100 $\mu$m) were obtained from Wilmad Glass. A single capillary was filled with deionized water, inserted into a 5 $\mu$l micropipette, sealed at the ends with wax, and inserted into a 2.5 mm i.d., 6-turn, transverse solenoid for NMR measurements.

Pulsed-field-gradient NMR measurements were performed using the ''13-interval, condition I'' alternating-direction (9), pulsed-gradient, stimulated-echo (*10, 11*) sequence combined with gradient prepulses and longitudinal storage before readout (*12, 13*) in order to avoid eddy-current-induced artifacts. A schematic of the pulse sequence is shown in Fig. 1. Spoiling gradient pulses orthogonal to the motion-encoding gradient pulses were applied during the two longitudinal storage periods. A 256-transient-phase cy-



1090-7807/97 $25.00

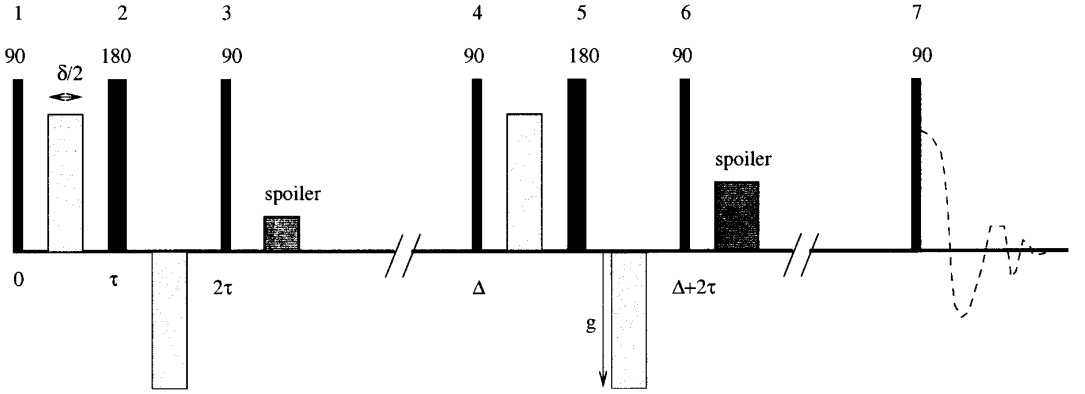


**FIG. 1.** ''13-interval, condition I'' pulse sequence (*9*) with longitudinal storage (*12*). The phase cycling employed involves 256 transients: a 128-transient cycle in which all seven RF pulses are cycled (the 90° pulses by 180° phase shifts and the 180° pulses by 90° phase shifts) plus an additional 128-transient sequence in which the phases of pulses 3 and 6 are shifted by 90° with respect to the first 128-transient sequence. In addition, gradient spoiling is applied during the longitudinal storage periods.

cle was used. Both 180° pulses were incremented by 90° while incrementing the receiver phase by 180°; 90° pulses were incremented by 180° while incrementing the receiver phase by 180°. In addition, the phase of the two storage pulses, pulses 3 and 6 in Fig. 1, were incremented by 90° while leaving the receiver phase constant in order to acquire signal corresponding to magnetization in the entire sample region. This latter phase cycling is essential for the ''13-interval, condition I'' sequence and the small sample used, since this sequence samples space as either $\cos^2(2\pi qz)$ or $\sin^2(2\pi qz)$, depending upon the relative phases of excitation and storage pulses.

Two sets of measurements were performed: one with pulsed field gradients oriented parallel to the capillary axis and one with gradients oriented perpendicular to the capillary axis, in the same direction as the applied static field. For gradients oriented parallel to the capillary axis, a single diffusion time, 1.003 s, was investigated. For gradients oriented orthogonal to the capillary axis, three separate diffusion times were investigated, 0.103, 0.503, and 1.003 s. For each diffusion time, the free-induction decay following the final radiofrequency pulse of the sequence shown in Fig. 1 was acquired for 32 values of the magnitude of the pulsed field gradient spaced linearly from 0 to 0.297 T/m. The resulting FIDs were Fourier transformed, and the resulting spectra were phase corrected, using a single zeroth-order phase correction for each diffusion time. After polynomial baseline correction, the absorption-mode spectra were integrated over the region of the water resonance peak to obtain measures of the stimulated-echo amplitudes.

Inversion-recovery measurements were performed on both the 100 $\mu$m i.d. capillary and on a 1 mm i.d. capillary filled with distilled water. Sixteen different recovery delays ranging from 1 ms to 7.0 s were used with a relaxation delay of 20 s. The resulting FIDs were processed as described above.

Figure 2 displays results from PFG NMR measurements with the pulsed field gradient oriented parallel to the capillary axis. These data indicate unrestricted diffusion since they agree well with the straight-line behavior on the semi-logarithmic plot of echo amplitude versus $q^2$ predicted by theory for diffusion in an infinite medium (*9, 14*). For the case of the ''13-interval, condition I'' pulse sequence employed in this work,

$$E(q,\Delta) = \exp\{-(2\pi q)^2 D[\delta^2(\Delta - \tau/2 - \delta/12)]\}. \quad [3]$$

Note that here we have neglected the effects of background gradients and have used definitions of $\delta$ and $\Delta$ consistent with the pulse sequence diagram shown in Fig. 1 and with Eq. [1] [these definitions differ from those in (9)]. Nonlinear least-squares regression of Eq. [3] to the data shown in Fig. 2 with the the initial echo amplitude (for $q = 0$) and

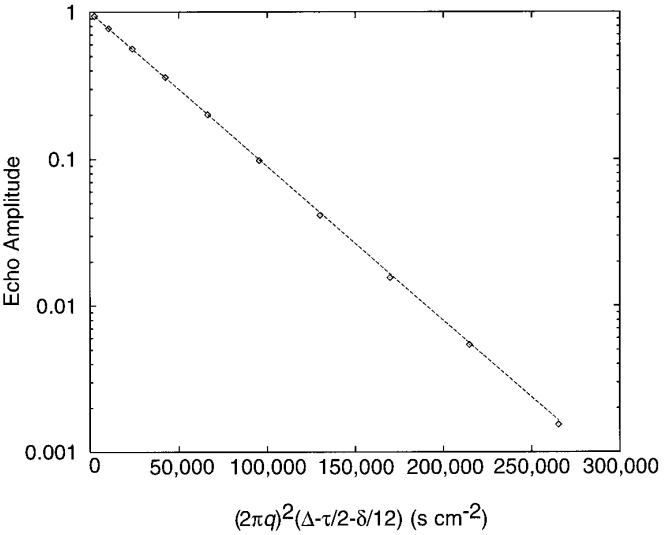


**FIG. 2.** Experimental data (points) and regression of Eq. [3] (line) for pulsed field gradients applied along the axis of a water-filled 50 $\mu$m i.d. capillary.

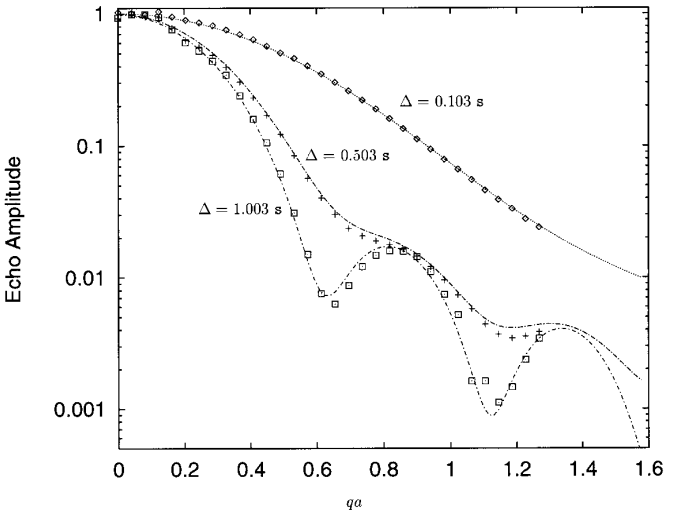


**FIG. 3.** Experimental data (points) and prediction of Eq. [1] (lines) for pulsed field gradients applied orthogonal to the axis of a water-filled 50 $\mu$m i.d. capillary for three different diffusion times corresponding to $D\Delta/a^2 = 0.098$, 0.48, and 0.96.

the diffusion coefficient as free-fitting parameters yields 2.42 $\pm$ 0.01 $\times 10^{-5}$ cm$^2$/s for the diffusion coefficient. This value is consistent with previously published values (*15*) at 25°C.

Analysis of the inversion-recovery data by nonlinear, least-squares regression of $A = A_0[1 - 2\alpha \exp(-\tau/T_1)]$ with $T_1$, $A_0$, and $\alpha$ as fitted parameters yielded $T_1$ values of 3.5 $\pm$ 0.05 s for water in the large diameter tube and 3.3 $\pm$ 0.03 s for water in the 100 $\mu$m capillary. These data suggest that the surface relaxivity of the capillary tube may be as large as 5 $\times 10^{-5}$ cm/s (*16*). Hence, the dimensionless parameter $Ma/D$, which plays an important role in Eqs. [1] and [2], is on the order of 0.01 for the water-filled 100 $\mu$m i.d. capillary; this value is effectively zero for conditions of interest.

Figure 3 shows results from PFG NMR measurements with the pulsed field gradient oriented orthogonal to the capillary axis for the three different diffusion times, $\Delta$. For comparison, the predictions of Eq. [1] with $a = 50$ $\mu$m and $D = 2.42 \times 10^{-5}$ cm$^2$/s and $M = 0$ are also shown. The agreement between the experimentally measured data and the predictions of Eq. [1] is best at mild attenuations of the echo. Possible causes of disagreement include nonorthogonality of the cylinder axis and the pulsed-gradient direction and inaccurate measurement of low echo amplitudes caused by incomplete correction of the spectra for broadline signals originating from immobile components of the probe. It is important to note that the lines shown in Fig. 3 are not fitted, but rather the predictions of Eq. [1] from independently determined parameters.

The striking features in Fig. 3 are the *diffractive* minima at long diffusion times, but Eq. [1] is also useful for investigating departures from the behavior for unrestricted diffusion predicted by Eq. [3] for small values of $q$ or $D\Delta/a^2$. Figure 4 shows a plot of $D_{app}/D$ versus $D\Delta/a^2$ obtained numerically from Eq. [1] from the initial slope of $\ln[E(q, \Delta)]$ versus $q^2$; here, $D_{app}$ is the apparent diffusion coefficient that one would determine by application of Eq. [3] to experimental data for small $q$. Also shown in Fig. 4 are lines representing the expected behavior at short and long diffusion times (or small and large values of $D\Delta/a^2$, respectively). At long diffusion times, the apparent diffusion coefficient of fluid restricted to the cylinder is $4a^2/\Delta$; at short diffusion times, the apparent diffusion coefficient is well represented by $D_{app}/D = 1 - (4/3a\sqrt{\pi})\sqrt{D\Delta}$, as suggested in (*7*). The global behavior may be approximately represented by $D_{app}/D = [1 + (4/3\sqrt{\pi})\sqrt{D\Delta/a^2} - 1.81(D\Delta/a^2)^{0.81} + 4(D\Delta/a^2)]^{-1}$, which has the correct limiting values for small and large $D\Delta/a^2$. It should be emphasized that Eq. [1] is valid for short gradient pulses; hence, we have not considered corrections to the effective diffusion time (*17*) for calculations shown in Fig. 4.

A common experimental configuration at the NHMFL employs a 2 mm diameter sample in a transverse solenoid for diffusion coefficient measurements. For small molecules, $D/a^2$ is on the order of 1 $\times 10^{-3}$ s$^{-1}$, and hence systematic errors of a few percent will occur in the measurement of diffusion coefficients for diffusion times $\Delta$ greater than 100 ms and pulsed gradients oriented orthogonal to the cylinder axis if experimental data are analyzed assuming unrestricted diffusion. In addition, the echo-attenuation behavior with increasing $q$ for this restricted geometry deviates mildly from the Gaussian behavior described by Eq. [3]. This deviation

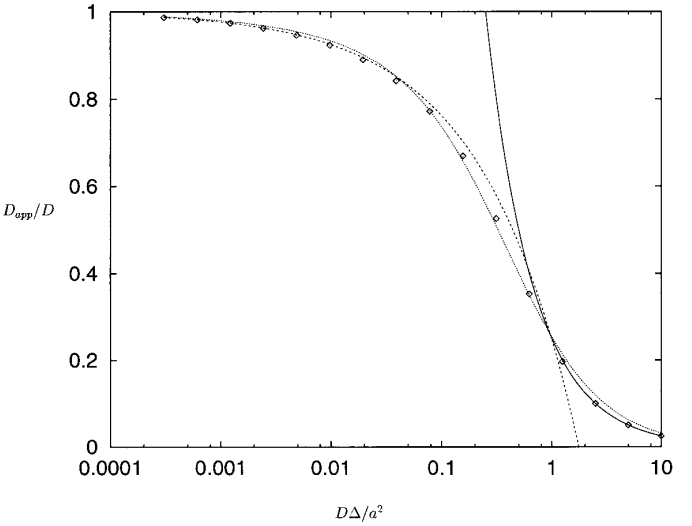


**FIG. 4.** Predictions of Eq. [1] (points) for the apparent diffusion coefficient of fluid entrapped in a cylinder of radius $a$ determined from small $q$ data with $q$ orthogonal to the axis of the cylinder. The dashed line shows $D_{app}/D = 1 - (4/3a\sqrt{\pi})\sqrt{D\Delta}$ and becomes negative for large $D\Delta/a^2$. The solid line represents the expected behavior for large $D\Delta/a^2$, $D_{app} = 4a^2/\Delta$, and the dotted line represents an approximate interpolation between these two limiting behaviors, $D_{app}/D = [1 + (4/3\sqrt{\pi})\sqrt{D\Delta/a^2} - 1.81(D\Delta/a^2)^{0.81} + 4(D\Delta/a^2)]^{-1}$.

will cause additional underestimation (for small $D\Delta/a^2$) of the diffusion coefficient from PFG measurements which will depend upon the range of $q$ values (or echo attenuations) sampled. For echo attenuations less than 100 and values of $D\Delta/a^2$ on the order of $1.0 \times 10^{-3}$, this latter effect is on the order of a few percent.

The experimental data presented above provide some confidence in the theoretical descriptions of PFG NMR in restricted geometries (*1*). In particular, experimental verification of the positions of *diffractive minima* in the PFG NMR data for restricted diffusion in a cylindrical geometry has been obtained. Detailed consideration of predictions of the theory (Eq. [1]) suggest caution in the interpretation of PFG data from fluids enclosed in millimeter-sized containers using theory developed for unrestricted diffusion.

## ACKNOWLEDGMENTS

This work was supported by the National High Magnetic Field Laboratory. The author is grateful for stimulating discussions with Drs. Bruce Locke, Timothy Moerland, Stephen Kinsey, and Chris Combs. The author also thanks the FAMU-FSU College of Engineering for providing computing resources.

## REFERENCES

1. P. T. Callaghan, *J. Magn. Reson. A* **113,** 53 (1995).
2. O. Sodderman, and B. Jonsson, *J. Magn. Reson. A* **117,** 94 (1995).
3. P. W. Kuchel, A. J. Lennon, and C. Durrant, *J. Magn. Reson. B* **112,** 1 (1996).
4. P. P. Mitra, P. N. Sen, and L. M. Schwartz, *Phys. Rev. B* **47,** 8565 (1993).
5. P. P. Mitra and P. N. Sen, *Phys. Rev. B* **45,** 143 (1992).
6. P. T. Callaghan, A. Coy, D. MacGowan, K. J. Packer, and F. O. Zelaya, *Nature* **351,** 467 (1991).
7. P. P. Mitra, P. N. Sen, L. M. Schwartz, and P. Le Doussal, *Phys. Rev. Lett.* **68,** 3555 (1992).
8. D. Cory and A. Garroway, *Magn. Reson. Med.* **14,** 435 (1990).
9. R. M. Cotts, M. J. R. Hoch, T. Sun, and J. T. Marker, *J. Magn. Reson.* **83,** 252 (1989).
10. E. L. Hahn, *Phys. Rev.* **80,** 580 (1950).
11. J. E. Tanner, *J. Chem. Phys.* **52,** 2523 (1970).
12. S. J. Gibbs and C. S. Johnson, Jr., *J. Magn. Reson.* **93,** 395 (1991).
13. E. J. Fordham, S. J. Gibbs, and L. D. Hall, *Magn. Reson. Imaging* **12,** 279 (1993).
14. E. O. Stejskal and J. E. Tanner, *J. Chem. Phys.* **42,** 288 (1965).
15. L. G. Longsworth, *J. Phys. Chem.* **64,** 1914 (1960).
16. K. R. Brownstein and C. E. Tarr, *Phys. Rev.* **19,** 2446 (1979).
17. E. J. Fordham, P. P. Mitra, and L. L. Latour, *J. Magn. Reson. A* **121,** 187 (1996).